iScience

CellPress
OPEN ACCESS

Article

Hierarchical partner selection shapes rod-cone pathway specificity in the inner retina

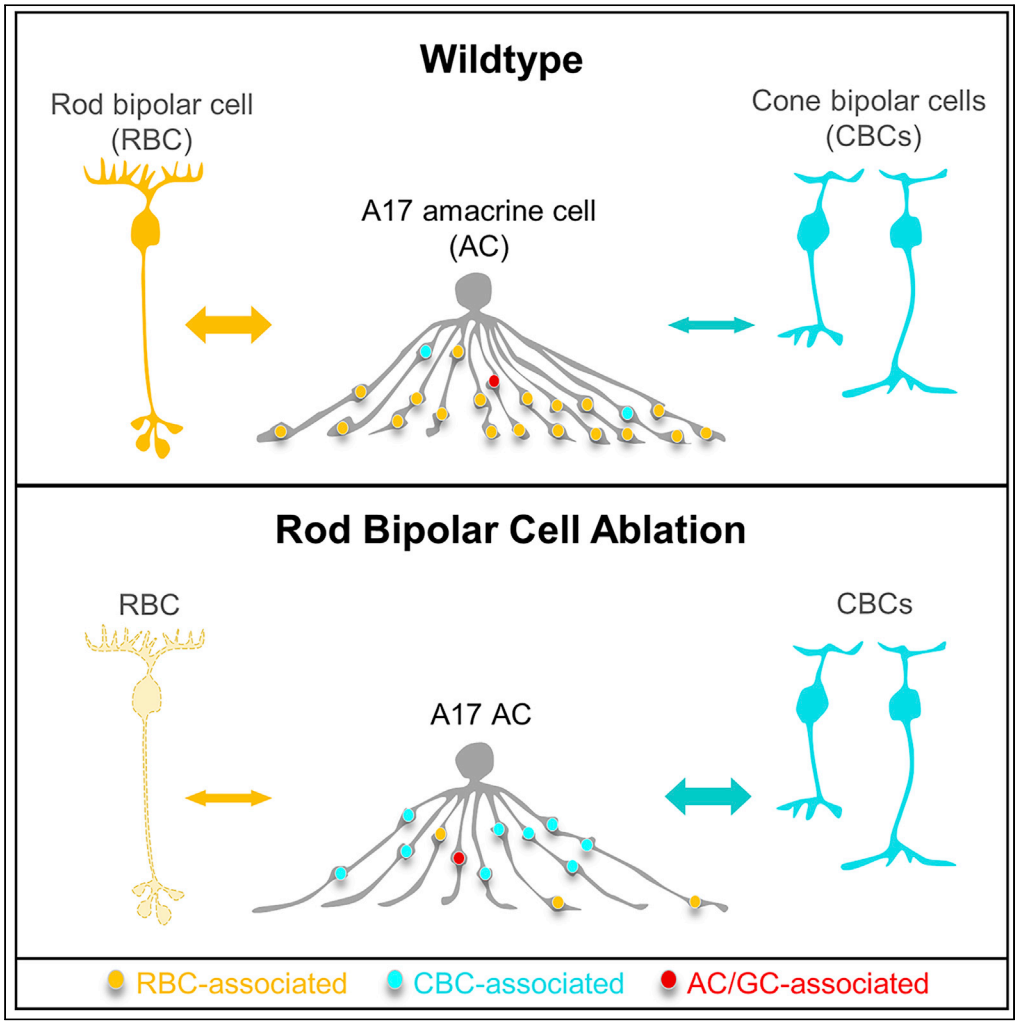

Chi Zhang, Ayana Hellevik, Shunsuke Takeuchi, Rachel O. Wong

wongr2@uw.edu

Highlights

A17s establish rod pathway-specific connectivity early during synaptogenesis

A17s engage both selective wiring and remodeling to shape their wiring pattern

A17s demonstrate a hierarchical choice of postsynaptic partners

A17s increase wiring with the cone pathway when rod bipolar targets are scarce

Zhang et al., iScience *25*, 105032
September 16, 2022
https://doi.org/10.1016/j.isci.2022.105032

iScience

CellPress
OPEN ACCESS

Article

Hierarchical partner selection shapes rod-cone pathway specificity in the inner retina

Chi Zhang,[1] Ayana Hellevik,[1] Shunsuke Takeuchi,[2] and Rachel O. Wong[1,3,*]

SUMMARY

Neurons form stereotyped microcircuits that underlie specific functions. In the vertebrate retina, the primary rod and cone pathways that convey dim and bright light signals, respectively, exhibit distinct wiring patterns. Rod and cone pathways are thought to be assembled separately during development. However, using correlative fluorescence imaging and serial electron microscopy, we show here that cross-pathway interactions are involved to achieve pathway-specific connectivity within the inner retina. We found that A17 amacrine cells, a rod pathway-specific cellular component, heavily bias their synaptogenesis with rod bipolar cells (RBCs) but increase their connectivity with cone bipolar cells (CBCs) when RBCs are largely ablated. This cross-pathway synaptic plasticity occurs during synaptogenesis and is triggered even on partial loss of RBCs. Thus, A17 cells adopt a hierarchical approach in selecting postsynaptic partners from functionally distinct pathways (RBC>CBC), in which contact and/or synaptogenesis with preferred partners (RBCs) influences connectivity with less-preferred partners (CBCs).

INTRODUCTION

In the vertebrate retina, the primary rod and cone pathways are composed of different cell types wired in distinct patterns. In the outer retina, rod photoreceptors mainly contact rod bipolar cells (RBCs), whereas cone photoreceptors wire with cone bipolar cells (CBCs) (Euler et al., 2014; Grimes et al., 2018; Masland, 2012; Wässle, 2004). RBCs (typically, a single type) and ON CBCs (multiple types) stratify within the ON sublamina of the inner plexiform layer (IPL) and depolarize in response to light increments, whereas OFF CBCs (multiple types) stratify within the OFF sublamina and have the opposite light response (Dunn and Wong, 2014; Hoon et al., 2014; Tsukamoto and Omi, 2017; Wässle, 2004; Zhang et al., 2017). CBCs directly synapse with ganglion cells (GCs), which are the output neurons of the retina, to transmit visual signals to the brain, whereas RBCs relay their information indirectly to GCs, by driving the responses of AII amacrine cells (ACs) that synaptically connect with both ON and OFF CBCs (Chun et al., 1993; Dunn and Wong, 2014; Grunert and Martin, 1991; Hoon et al., 2014; Pourcho and Goebel, 1985; Strettoi et al., 1990; Tsukamoto et al., 2001; Tsukamoto and Omi, 2017; Wässle, 2004). Furthermore, neurotransmission from RBCs and CBCs is modulated by inhibition from a diversity of ACs (Hoon et al., 2014; Wässle, 2004; Yan et al., 2020). The assembly of rod and cone connectivity in the outer retina appears to involve different molecular mechanisms and dependency on visual experience (Cao et al., 2015, 2020; Dunn et al., 2013; Maddox et al., 2020), suggesting that rod and cone connections may be wired independently. Whether rod and cone pathway connectivity within the inner retina are also wired by distinct mechanisms during development is unknown. Gaining this knowledge is not only important for a more complete understanding of how these two parallel pathways of the visual system are established but also whether cross-pathway connections are potentially possible in the reassembly of photoreceptor circuits during repair.

A17 ACs in the inner retina are critical for rod pathway signaling, because they modulate and synchronize light-driven RBC responses across the retina (Grimes et al., 2010, 2014, 2018). Although the neurites of A17 ACs traverse the full depth of the IPL, A17s are thought to be rod pathway-exclusive and not contact CBCs (Chun et al., 1993; Freed et al., 1987; Grunert and Martin, 1991; Hartveit, 1999; Kolb and Famiglietti, 1974; Nelson and Kolb, 1985; Raviola and Dacheux, 1987; Sandell et al., 1989; Tsukamoto et al., 2001). Previous studies showed that the varicosities of A17 ACs form synaptic dyads together with AII ACs as apposed to RBC axonal ribbons in the ON sublamina, while making GABAergic reciprocal synapses onto RBCs to provide inhibitory modulation (Figures 1A–1C) (Freed et al., 1987; Grimes et al., 2014; Kolb and Famiglietti, 1974; Massey et al., 1992; Pourcho

[1]Department of Biological Structure, University of Washington, Seattle, WA 98195, USA

[2]Department of Biological Sciences, University of Tokyo, Tokyo 113-0033, Japan

[3]Lead contact

*Correspondence: wongr2@uw.edu

https://doi.org/10.1016/j.isci.2022.105032

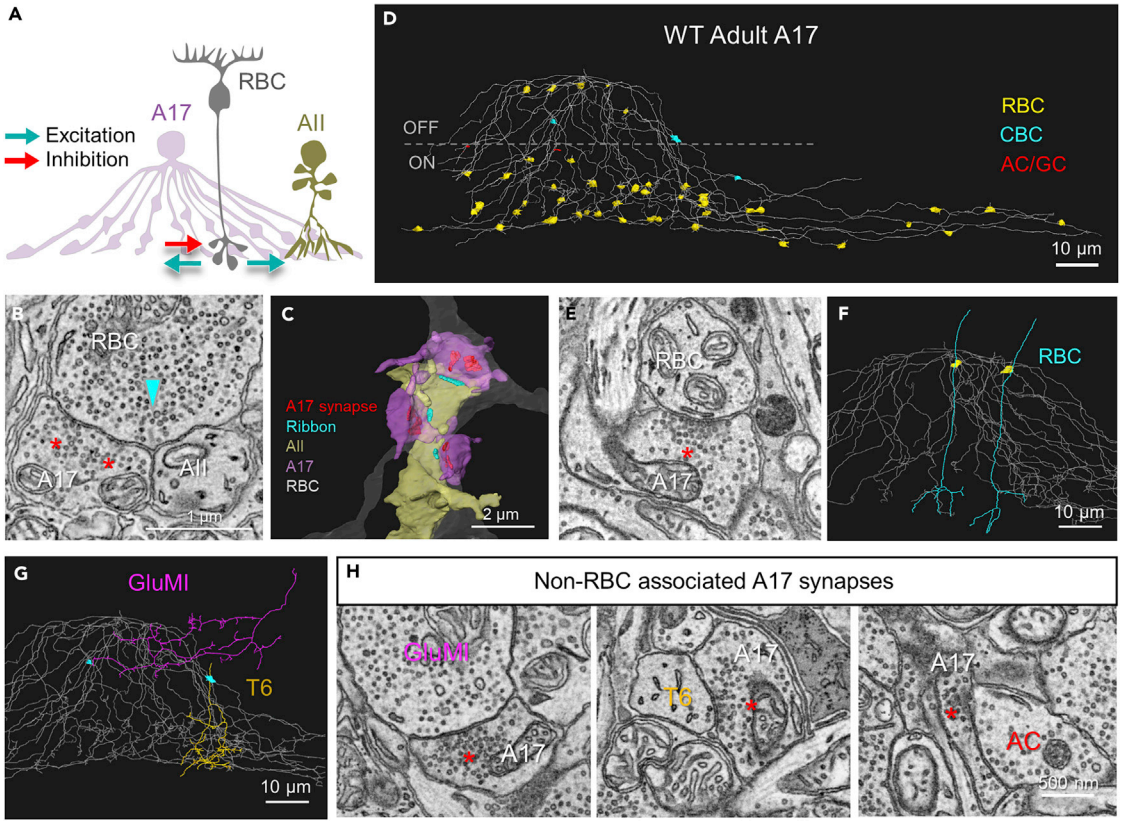

Figure 1. Wild-type adult A17 amacrine cells predominantly synapse with rod bipolar cells

(A) Schematic diagram of the circuit formed by an A17 amacrine cell (AC) and an AII AC with the axon terminal of a rod bipolar cell (RBC).

(B) Electron micrograph showing an adult wild-type (WT) RBC-AII/A17 dyad synapse. RBC ribbon is indicated by a cyan arrowhead. This A17 bouton makes two reciprocal inhibitory synapses (red asterisks) with the RBC.

(C) Three-dimensional (3D) SBFSEM reconstruction of three A17/AII-RBC dyads, with A17 reciprocal synapses (red) indicated.

(D) 3D reconstruction (skeleton) of a WT adult A17 showing the partner types and locations of its output synapses. CBC, cone bipolar cell; GC, ganglion cell; AC, amacrine cell.

(E) Electron micrograph of a non-reciprocal A17 synapse (red asterisk) at an RBC axon shaft.

(F) Axonal skeletons of two RBCs receiving non-reciprocal synaptic contacts at their axon shafts from the A17 in panel C, with the associated A17 synaptic varicosities indicated in yellow.

(G) Skeletons of a GluMI CBC and a type 6 (T6) ON CBC postsynaptic to the A17 in panel D, with the associated synaptic varicosities indicated in cyan.

(H) Representative electron micrographs of non-RBC associated A17 synapses. Red asterisks indicate A17 synapses.

and Goebel, 1985; Raviola and Dacheux, 1987; Sinha et al., 2020; Strettoi et al., 1990; Tsukamoto and Omi, 2017). How A17 ACs primarily target RBCs and establish their partnership in RBC dyads during development are unknown. Given their highly specific connectivity pattern, one plausible strategy is that A17 ACs are "hard-wired" with RBCs as early as synaptogenesis and never connect with the cone pathway. Alternatively, A17 ACs non-selectively contact rod and cone pathway neurons during development with their widespread processes and undergo remodeling to attain their rod pathway specificity. To distinguish between these possibilities, we used correlative fluorescence imaging and serial block-face scanning electron microscopy (SBFSEM) to reconstruct the morphology and synaptic arrangements of A17 ACs in normal neonatal and adult mouse retina, and in animals where RBCs were largely ablated during development.

RESULTS

A17 amacrine cells predominantly synapse with rod bipolar cells

To determine the synaptic wiring pattern of individual A17s in more detail, we reconstructed adult wild-type (WT) mouse A17s from two SBFSEM volumes. For each reconstructed A17 AC, we mapped all its output synapses and identified the associated postsynaptic cell types. Each A17 synapse we observed was with a single postsynaptic partner (n = 3 cells, 506 synapses in total). Consistent with previous studies

Table 1. Summary of WT adult A17 AC synaptic arrangements

	Synaptic partner types						
	RBC		CBC				
Cell ID	R	Non-R	R	Non-R	AC	GC	Total
WT-A17-1	114	18	3	2	2	0	139
WT-A17-2	108	36	5	0	3	1	153
WT-A17-3	187	21	2	2	2	0	214
%	95.4 ± 0.9		2.9 ± 0.5		1.7 ± 0.5		100

RBC, rod bipolar cell; R, reciprocal synapse; CBC, cone bipolar cell; AC, amacrine cell; GC, ganglion cell.
Data are shown as mean ± SEM.

(Grimes et al., 2014; Sinha et al., 2020; Tsukamoto et al., 2001), A17s preferentially synapsed with RBCs (95.4 ± 0.9%; Figure 1D).

The majority of RBC-associated A17 synapses were located nearby a ribbon synapse of an RBC axon terminal or shaft in the ON sublamina. 83.8 ± 4.5% of these synapses were reciprocal feedback connections (Figures 1B and 1C; Table 1). The remainder of the RBC-associated A17 synapses were non-reciprocal and were often made onto RBC axonal shafts in the OFF sublamina (Figures 1E and 1F).

We also found that a small fraction of adult A17 synapses were made with CBCs, other ACs, and GCs (Figures 1G and 1H; Table 1). All three A17s we reconstructed contacted GluMI CBCs (Della Santina et al., 2016) and one A17 also contacted Type 6 (T6) ON CBCs (Figures 1G and 1H) (Tsukamoto and Omi, 2017). The CBC-associated A17 synapses also involved reciprocal and non-reciprocal synapse arrangements (Table 1). The AC targets included AII ACs and some wide-field ACs. Overall, WT A17 ACs predominantly contact RBCs, with only a few exceptions.

A17 amacrine cells bias synaptogenesis with rod bipolar cells during development

To determine how A17s achieve their RBC-dominant connections, we reconstructed the connectivity patterns of developing A17s (Figures 2A-2C). Previously (Schubert et al., 2008), we found that RBCs receive functional GABAergic input around postnatal days (P) 8-9. We thus first examined the connectivity of A17s at P9. Compared to their adult counterparts, P9 A17s were morphologically immature with fewer radiating long processes (Figures 2A and S1). They did not yet exhibit varicosities along their processes, although many output synapses were apparent (n = 3 cells, 180 synapses). The preference for RBCs was already evident at P9. About 80% of the A17 synapses were made with RBCs, whereas CBC-associated synapses were rarely seen (Figures 2A and 2C). Only 1 out of the 3 reconstructed cells had a CBC-associated synapse (Table 2). However, compared to the adult, at P9 there was a significantly higher percentage of A17 synapses targeting ACs or GCs (Figure 2C).

By P11, a few days before eye opening, the morphology of A17s resembled that of mature ACs, showing more radiating processes and prominent varicosities at which synapses were observed (Figures 2B and S1; n = 4 cells, 346 synapses). Consistent with the change in morphology, we found more RBC-associated synapses from each P11 A17 AC than their P9 counterparts (Table 2), despite the EM volume and reconstructed A17 arbors of the P11 retina being less complete than the ones of the P9 retina (Figure S1; STAR Methods). As a result, there was an increase in the percentage of RBC-associated synapses compared to P9. This percentage at P11 was similar to that of the adult (Figure 2C). In contrast, the fraction of synapses associated with CBCs remained unchanged and connections with AC/GCs decreased at P11 (Figure 2C). Of the 4 reconstructed P11 cells, we did not observe any CBC-associated synapses in 3 cells or AC/GC-associated synapses in 2 cells (Table 2). Therefore, A17s already prefer RBCs as their major synaptic partner at the early stages of synaptogenesis before visual experience occurs. As A17s mature, they eliminate synapses with ACs and GCs to connect almost exclusively with RBCs (Figure 2C).

A17 amacrine cells are not required to initiate rod bipolar cell dyad assembly

Although A17s prefer RBCs as their primary targets, they are also the major postsynaptic partners of RBCs. Consistent with previous measurements (Sinha et al., 2020), we found that most adult RBC axonal ribbons

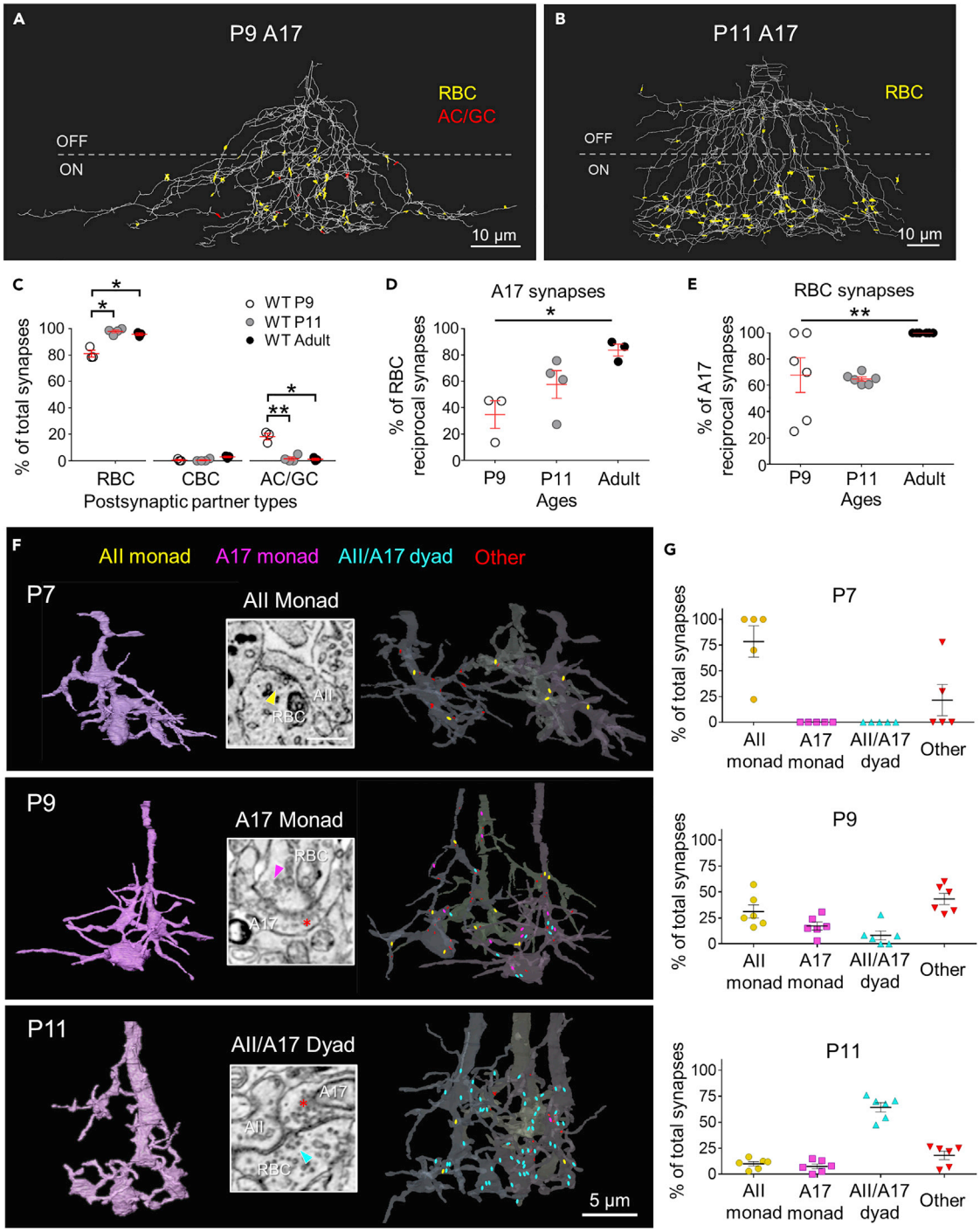

Figure 2. Development of A17 AC-associated synapses

(A) WT postnatal day (P) 9 A17 arbor and synapses color-coded according to postsynaptic cell types.

(B) A WT P11 A17 and synapses.

(C) Proportions of A17 synapses associated with different postsynaptic partner types in P9, P11, and adult WT retina (n = 3, 4, and 3 cells, respectively; Unpaired t-test).

(D) Percentage of A17 synapses with RBCs that are associated with an RBC ribbon increases with maturation (Kruskal-Wallis test).

(E) Percentage of RBC ribbon synapses that have A17 reciprocal input increases with age (P9, n = 6 cells; P11, n = 6; Adult, n = 6; Kruskal-Wallis test).

Figure 2. *Continued*

(F) 3D reconstructions of P7, P9, and P11 RBCs with their synapses identified. Locations of AII monads, A17 monads, and A17/AII monads are color-coded according to synapse type. Synapses associated with GCs and/or non-AII/A17s are in red (other). Representative electron micrographs of each synapse arrangement are provided. Arrowheads indicate ribbons, color-coded by synapse arrangement type. Red asterisks indicate A17 reciprocal synapses.
(G) Percentages of WT RBC synapses with different synaptic arrangements in P7, P9, and P11 retina. Data are shown as mean ± SEM. *, $p < 0.05$; **, $p < 0.01$; n.s., not significant. See also Figures S1 and S2.

were apposed to AII/A17 at dyads (91.7 ± 1.8%, n = 6 cells). From P9 onwards, we observed an increase in the percentage of A17 reciprocal synapses with RBCs (Figure 2D). This raised the possibility that during the assembly of RBC dyad synapses, RBC ribbons appear after A17s synapse onto RBC axons. To test this hypothesis, we analyzed the synaptic arrangement of developing RBCs at P7, P9, and P11 (Figures 2F and 2G; n = 5, 6, 6 cells respectively). RBCs can be recognized as early as P7 by their lobular axonal morphology and stratification within the innermost level of the IPL (Figure 2F). Unlike in adult (Sinha et al., 2020; Sterling and Matthews, 2005), synaptic ribbons were not observed within P7 or P9 RBC axons. Instead, they had densely clustered vesicles as opposed to thickened cell membranes, suggesting the location of active zones (Figure 2F). At P11, there were spherical structures with vesicles tethered, likely representing proto-ribbons (Figure 2F). Synapse numbers per RBC increased significantly with age (P7, 5 ± 2; P9, 24 ± 3; P11, 35 ± 3; $p < 0.0001$; Kruskal Wallis test).

Contrary to our hypothesis, A17s were not present at any RBC synapse until P9 (Figure 2G). Moreover, at P9 and P11, not all the A17s postsynaptic to RBCs made reciprocal feedback synapses (Figure 2E). Therefore, RBC dyad assembly is not initiated by A17 synapsing with RBCs. In fact, most early RBC synapses at P7 were associated with AII ACs (Figure 2G), which could be identified by their morphology (Figure S2) (Gamlin et al., 2020). A17s, however, did not depend on AIIs to participate in dyad assembly, because both AII and A17 monads were present at P9 and P11 (Figure 2G). Consistent with our earlier finding (Morgan et al., 2011), RBCs also made synapses with GCs or non-AII/A17s during development (Figures 2F and 2G), which were likely eliminated upon maturation. Taken together, these observations suggest that there is not a fixed sequence in the assembly of RBC dyads, where one specific postsynaptic partner dictates the location of the future dyad.

A17 amacrine cells target cone bipolar cells when rod bipolar cells are reduced in availability during development

The robust connectivity between A17s and RBCs in the adult and during development implicates a "classic" mechanism that specifically partners these two cell types, perhaps involving molecular cell-cell recognition cues (Sanes and Zipursky, 2020), throughout synaptogenesis. If so, we would predict that A17s will not increase synaptogenesis with other neurons if RBC partners were scarce. To test this hypothesis, we determined the connectivity pattern of A17s in mice after genetically ablating large numbers of RBCs during development. We did not ablate all RBCs because we depended on contact between A17s and some RBCs to identify and trace the A17 arbors. We bred *αPax6-Cre* with *Grm6-YFP-STOP-DTA* mice (DTA mice) to generate retinas in which outside a dorsal-ventral strip, most RBCs as well as many T6, some T7, and T8 ON CBCs were ablated upon diphtheria toxin A (DTA) expression before A17 and BC synaptogenesis (Figure 3A) (Marquardt et al., 2001; Morgan et al., 2011; Okawa et al., 2014). The majority of the remaining RBCs in the DTA retina were YFP-positive. We used correlative light and electron microscopy (Bishop et al., 2014) to acquire EM reconstructions from regions where only a few YFP-positive RBCs were observed (Figures 3B and 3C; STAR Methods). This enabled us to trace A17s from contacts with the remaining RBCs (Figure 3D).

Three adult A17s were reconstructed from a DTA retina (Figures 3E and S3A), with all their synapses and postsynaptic cells identified (133 synapses in total; Table 3). Unlike adult WT A17s, DTA A17s no longer densely made synapses in the ON sublamina, presumably owing to a lack of RBCs (Figure 3E). Instead, DTA A17s synapsed with a diversity of ON and OFF CBC types throughout the depth of the IPL (Figures 3E and 3F). Compared to WT, DTA A17s had a higher percentage of synapses made with CBCs (Figure 3H). This increase in CBC connectivity was not caused simply by a decreased number and percentage of RBC-associated synapses. Although we were only able to quantify synapses of each A17 within the EM volume, each DTA A17 did make more synapses with CBCs compared to WT (Tables 1 and 3), even though the EM volume of the DTA retina was smaller than the WT volumes (STAR Methods). Like their WT counterparts, a proportion (31.5 ± 5.7%) of CBC-associated DTA A17 synapses were reciprocal (Figures 3G and 3G′). Furthermore, a few A17 synapses (5 out of 133 synapses) Involved varicosities that

Table 2. Summary of developing A17 AC synaptic arrangements

	Synaptic partner types			
Cell ID	RBC	CBC	AC/GC	Total
P9-A17-1	51	0	8	59
P9-A17-2	51	1	13	65
P9-A17-3	44	0	12	56
%	81.2 ± 2.6	0.5 ± 0.5	18.3 ± 2.4	100
P11-A17-1	136	0	0	136
P11-A17-2	55	1	0	56
P11-A17-3	75	0	1	76
P11-A17-4	74	0	4	78
%	97.9 ± 1.1	0.4 ± 0.4	1.6 ± 1.2	100

Data are shown as mean ± SEM

formed dyads with AII AC lobular appendages at CBC ribbon sites in the OFF sublamina, recapitulating the arrangement of RBC dyads (Figure S3B). Compared to CBCs, other ACs and GCs remained the minor partners of A17s in the DTA retina (Figure 3H). Thus, A17s have the capacity to make synapses not only across sublaminae in the IPL but also with both ON and OFF types of CBCs. Moreover, the ablation of RBCs unmasked a hierarchy for partner selection by A17s, which prioritizes BCs amongst partner classes and RBCs among BC types.

Is the increase in connectivity with CBCs when RBCs are scarce owing to selective synaptogenesis or a result of exuberant early connections that are pruned over time, such as that which occur in other neural circuits (Kano and Watanabe, 2019; Liang and Chen, 2020; Morgan et al., 2011)? To answer this question, we determined the connectivity pattern of A17s in the DTA retina at P10, when A17-RBC synaptogenesis is ongoing (Figure 2). Given that the level of DTA expression varies across individual mice and retinal locations, we noted that the P10 area we examined had about half of the RBCs ablated (Figure 4A). In this area, four A17s were reconstructed (Figure 4B). Not surprisingly, P10 A17s are wired with RBCs within their vicinity with decent numbers of synapses (Figures 4C and 4D; Table 4). However, these A17s also formed a significant number of synapses with CBCs, increasing the percentage of such synapses compared to their WT counterparts at P9 and P11 (Figure 4C). Similar to our observations in the DTA adult retina, both ON and OFF CBCs were the targets of DTA P10 A17s (Figure 4D). DTA P10 A17s, however, synapsed with ACs and GCs at a similar frequency to WT P9 cells (Figure 4C). Like WT, these synapses with AC/GCs are likely to be eliminated by adulthood (Figure 3H). Together, our observations suggest that A17s selectively increase synaptogenesis with CBCs and that partial loss of RBCs during development is sufficient to promote this process.

DISCUSSION

Synaptogenesis of A17 amacrine cells is biased toward rod bipolar cells early in development

Using SBFSEM, we identified the cell types postsynaptic to A17 ACs in the mature and developing mouse retina. Consistent with previous findings (Freed et al., 1987; Nelson and Kolb, 1985), adult A17 ACs predominantly synapse with RBCs. We also found that A17 ACs synapse with CBCs, ACs, and GCs, but these connections constituted a negligible fraction of the total number of output synapses made by the A17 cells. A17 ACs' biased connectivity with RBCs emerges early in development before visual experience occurs, and A17 ACs maintain this connectivity bias by gradually adding synapses with RBCs and pruning synapses with AC/GCs throughout development. Such early biases in synaptic wiring have also been observed in other inhibitory interneurons, such as the H3 horizontal cell in the zebrafish retina, which prefers UV over blue cones, and the chandelier cell in mouse cortex which make synapses exclusively at the axon initial segment of pyramidal neurons (Steinecke et al., 2017; Yoshimatsu et al., 2014). Together with these past observations, our current findings underscore a cellular strategy for selecting a preferred synaptic partner that differs from mechanisms that gradually shape connectivity through massive circuit remodeling.

Our current measurements confirm previous observations that the vast majority of A17 synaptic varicosities form characteristic synaptic dyads together with AII ACs at RBC ribbon sites (Grimes et al., 2014; Sinha

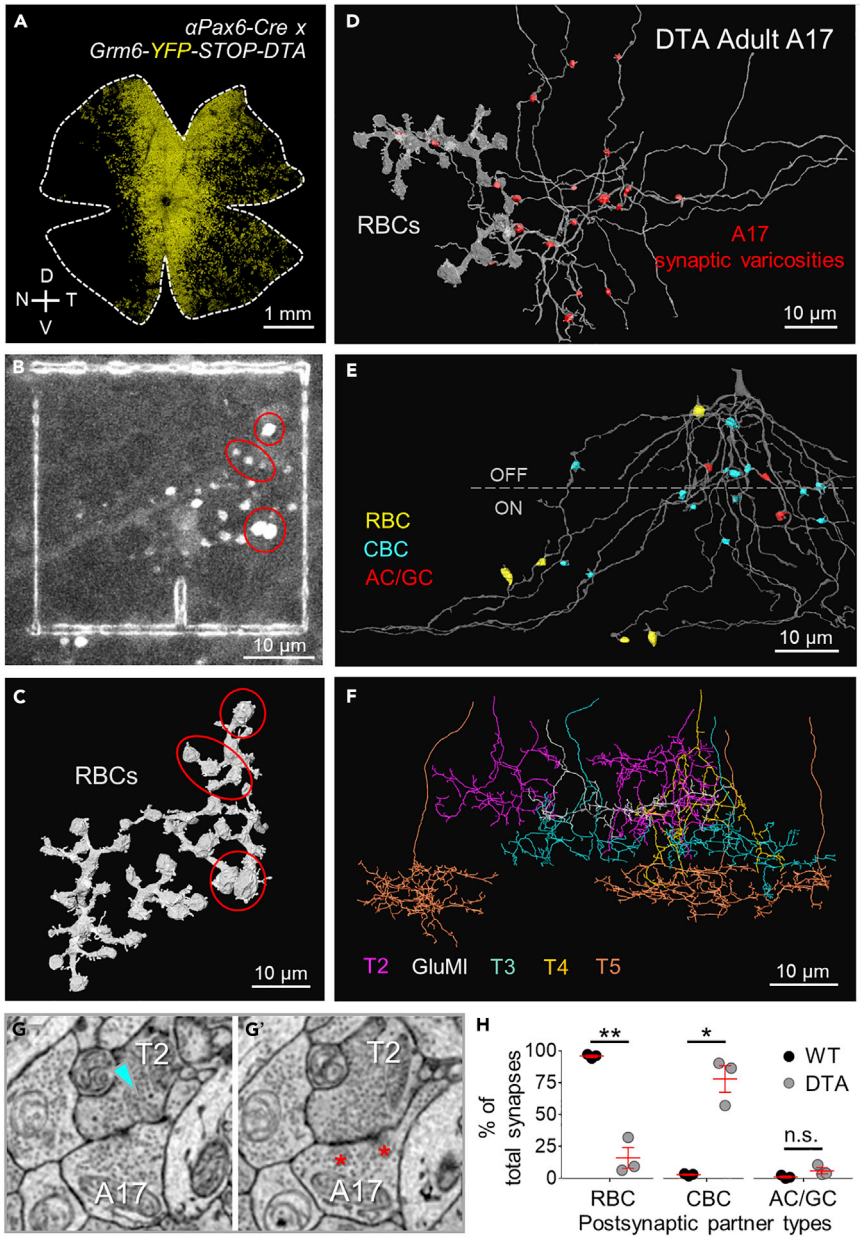

Figure 3. A17 ACs synapse with many ON and OFF CBCs when RBCs are largely absent

(A) Representative fluorescence image of a retinal whole mount from *αPax6-Cre x Grm6-YFP-STOP-DTA* (DTA) mice. The edge of the retina is outlined by a dashed line. D, dorsal; V, ventral; N, nasal; T, temporal.

(B) Two-photon image of the area in the adult DTA retina selected for SBFSEM, showing fiducial marks made by near-infrared branding. Axons of some remaining RBCs are indicated by red ovals.

(C) 3D reconstructions of all the remaining RBCs within the acquired EM volume. Red ovals indicated the same axonal structures indicated in panel B.

(D) A representative A17 synaptically connected to the remaining RBCs, with all its synaptic boutons labeled in red.

(E) The A17 in panel D with the output synapses color-coded according to postsynaptic cell type.

(F) All the CBCs postsynaptic to the A17 in panel D.

(G) Two consecutive electron micrographs show an OFF CBC-A17 reciprocal synapse. Cyan arrowhead, ribbon; red asterisk, A17 synapse.

(H) Proportions of A17 synapses with different partners in adult WT and DTA retina (n = 3 cells each; unpaired t-test). Data are shown as mean ± SEM. *, $p < 0.05$; **, $p < 0.01$; n.s., not significant. See also Figure S3.

Table 3. Summary of DTA adult A17 AC synaptic arrangements

	Synaptic partner types						
	RBC		CBC				
Cell ID	R	Non-R	R	Non-R	AC	GC	Total
DTA-A17-1	7	2	4	12	3	0	28
DTA-A17-2	2	0	12	16	1	0	31
DTA-A17-3	3	4	19	45	3	0	74
%	16.0 ± 8.1		78.0 ± 10.5		6.0 ± 2.4		100

Data are shown as mean ± SEM.

et al., 2020; Tsukamoto and Omi, 2017). By following the development of the RBC dyad, we found that AII and A17 ACs do not depend on each other or follow a strict temporal sequence to be recruited at RBC ribbons. Furthermore, there are very few instances where more than one A17 or AII process is apposed to a RBC ribbon during development, indicating that A17 or AII ACs do not "compete" with their own types at a synaptic site. Interestingly, A17 varicosities and AII lobular appendages in the OFF sublamina can form dyads at CBC ribbon sites when RBCs are scarce. This suggests a mechanism for A17-AII dyad formation that is independent of IPL depth and specific bipolar cell types.

Mechanisms that determine the wiring specificity of A17 amacrine cells

Neural circuits employ various molecular mechanisms to achieve wiring specificity (Sanes and Zipursky, 2020). Neuronal partners are often guided by attractive and repulsive molecular cues to elaborate axons and dendrites within the right locations to facilitate physical contact and synaptogenesis. For example, retinal neurons stratify within separate sublayers of the IPL to form the ON vs. OFF pathways. But, despite having neurites that traverse the entire depth of the IPL, A17 ACs make the vast majority of their output synapses within the ON sublamina with RBCs. This suggests that the wiring pattern of A17s is unlikely owing to a constraint of laminar-restricted cues, but instead, is dictated by a preference for RBCs as the primary target. It is also unlikely that A17 ACs restrict output synaptogenesis to their distal processes, like starburst amacrine cells (Briggman et al., 2011; Ding et al., 2016), because A17 ACs also synapse with RBC axon shafts in the OFF sublamina.

Besides limiting the location and region of their processes for synaptogenesis, neurons also depend on molecular interactions to recognize and recruit specific synaptic partners to establish their appropriate connectivity pattern. Our results show that a simple cell-cell recognition cue between A17 ACs and RBCs does not account fully for specificity in connectivity between these two cell types. Instead, A17 ACs demonstrate a hierarchy for partner selection, which prioritizes BCs across cell classes and RBCs amongst BC types. This hierarchy may be established by different expression levels or by different combinations of recognition molecules (e.g. adhesion molecules) at A17 contacts with RBCs, CBCs, and AC/GCs. Such hierarchy in synaptic partner choice has also been observed in drosophila and zebrafish (Xu et al., 2019; Yoshimatsu et al., 2014), but A17s represent the first example of inhibitory neurons demonstrating a synaptogenic hierarchy for establishing presynaptic inhibition.

Cross-pathway wiring plasticity of A17 amacrine cells

The visual system across invertebrates and vertebrates shares a common feature—numerous types of neurons are wired in stereotypic patterns to form visual circuits that perform specific functions. Different visual circuits, however, use diverse wiring strategies. For instance, drosophila visual pathways from the retina to the optic lobe are genetically "hard-wired" with precise cell types and numbers which do not require synaptic pruning (Neriec and Desplan, 2016; Sanes and Zipursky, 2020). In contrast, the retinogeniculate pathways in mammals depend not only on molecules but also on spontaneous and visual activity that direct large-scale synaptic pruning to shape eye-specific and retinotopic connections (Liang and Chen, 2020). Distinct from these two highly contrasting scenarios, A17 ACs are likely molecularly programmed to wire exclusively in the rod pathway, but also experience moderate synaptic pruning to remove non-BC synapses. Furthermore, A17 ACs demonstrate plasticity that is independent of visual activity to connect to both ON and OFF cone pathways, when rod pathway neurons (RBCs) are sparser than usual. The cross-pathway plasticity of A17 ACs is highly robust, because A17 ACs quickly synapse with

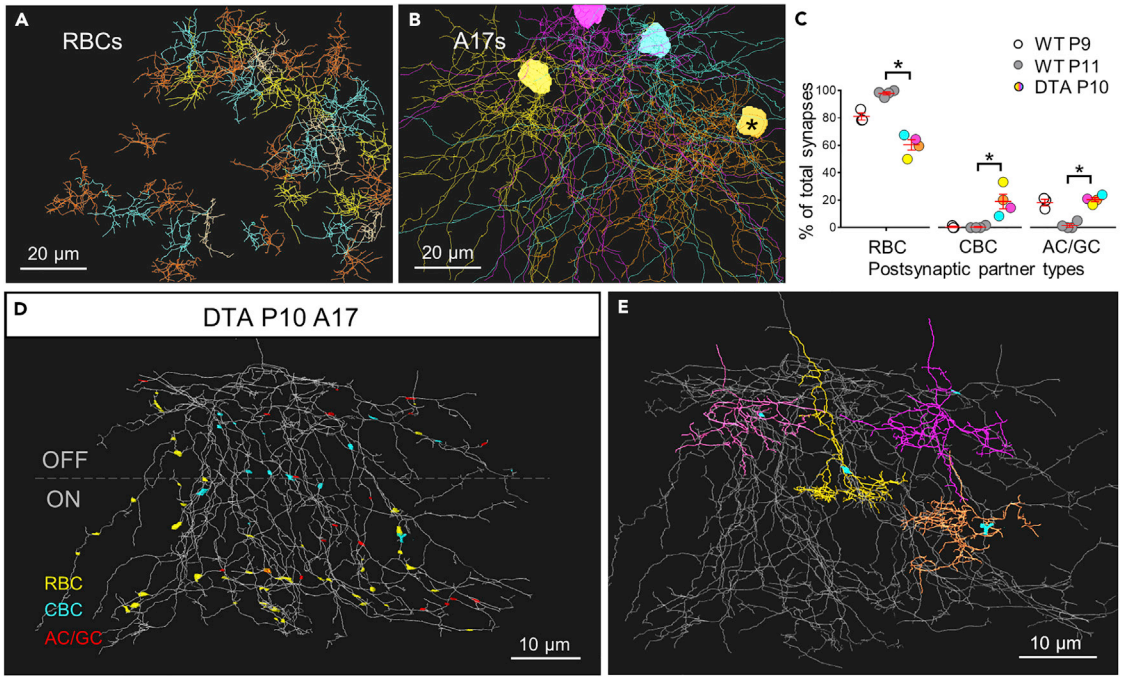

Figure 4. A17 ACs make more synapses with CBCs as early as synaptogenesis when RBCs are sparse

(A) Axonal skeletons of all the remaining RBCs in the acquired EM volume of a P10 DTA retina.

(B) Skeletons of the A17 arbors analyzed in the P10 DTA retinal volume. The asterisk indicates the A17 in panels D and E.

(C) Distributions of A17 synapses across different synaptic partners in WT P9, P11, and DTA P10 retina (n = 3, 4, and 4 cells; unpaired t-test). The color-coded data points of the DTA retina correspond to the colored A17s in panel B.

(D) An A17 (indicated by the asterisk in panel B) and its synaptic boutons color-coded according to the contacted postsynaptic cell type. E. Representative CBC types contacted by the A17 in panel D with their associated synaptic boutons labeled in cyan. Data are shown as mean ± SEM. *, $p < 0.05$.

more CBCs when RBCs are partially ablated during development. Therefore, for A17 ACs, making more synapses appears to be of greater priority than wiring only with the right synaptic partners. However, A17 ACs maintained their synaptic arrangement with RBCs—in the DTA retina, the A17 formed a single bouton at each contact site with the surviving RBCs, characteristic of the wild-type arrangement. Moreover, the aberrant CBC-associated A17 synapses often recapitulate the dyad arrangement at RBC axons. Thus, the A17 AC does not compensate for the loss of RBCs by altering the structural arrangement of its varicosities, each of which represents a functionally independent unit (Grimes et al., 2010), but instead forms novel connections with CBCs.

Cross-pathway wiring plasticity during development has been observed in outer retinal circuits. For instance, mouse RBCs synapse with cone-like cells when rods are absent (Keeley and Reese, 2010). Fish H3 cells connect with significantly more blue cones when UV cones are absent. Our current observations emphasize that the primary rod/cone pathways are not wired independently during development, showing that rewiring can occur in the inner retina involving an inhibitory interneuron normally dedicated to the rod pathway. Whether loss of CBCs causes an increase in CBC-preferring ACs to wire with RBCs will need to be explored in the future in order to determine whether rod-cone cross-pathway rewiring is bidirectional. Together with our current findings, these future experiments will have important implications for restoring specificity in rod-cone pathway connections in retinal circuit repair.

Limitations of the study

Our study demonstrates a hierarchical partner selection mechanism that determines the wiring specificity of A17 ACs, as well as their rod-cone cross-pathway plasticity. Elucidation of the molecular mechanisms responsible for A17 wiring specificity and plasticity will require the future availability of transgenic mouse lines that specifically label A17 ACs and knowledge of the molecular profile of these cells.

Table 4. Summary of DTA P10 A17 AC synapse arrangements

	Synaptic partner types			
Cell ID	RBC	CBC	AC/GC	Total
DTA-A17-1	59	20	20	99
DTA-A17-2	48	6	17	71
DTA-A17-3	49	11	16	76
DTA-A17-4	25	15	8	48
%	60.4 ± 3.8	19.1 ± 5.3	20.5 ± 1.5	100

Data are shown as mean ± SEM.

STAR★METHODS

Detailed methods are provided in the online version of this paper and include the following:

- KEY RESOURCES TABLE
- RESOURCE AVAILABILITY
  - Lead contact
  - Materials availability
  - Data and code availability
- EXPERIMENTAL MODEL AND SUBJECT DETAILS
  - Mice
- METHOD DETAILS
  - Retinal tissue preparation and fixation
  - Confocal image acquisition and processing
  - Correlative light and electron microscopy
  - Serial block-face scanning electron microscopy (SBFSEM)
  - Image reconstruction and analysis
- QUANTIFICATION AND STATISTICAL ANALYSIS

SUPPLEMENTAL INFORMATION

Supplemental information can be found online at https://doi.org/10.1016/j.isci.2022.105032.

ACKNOWLEDGMENTS

Supported by NIH grant EY-10699 and EY-17101 to R.O. Wong, and the Vision Core grant EY01730 to M. Neitz. Graduate Research Abroad in Science Program (GRASP) of The University of Tokyo and Graduate Program for Leaders in Life Innovation (GPLLI) to S. Takeuchi. We thank Sharm Knecht, Ed Parker, and Dale Cunningham for technical assistance with electron microscopy. We thank Mike Ahlquist for the assistance with electron microscopy image segmentation.

AUTHOR CONTRIBUTIONS

Conceptualization, C.Z. and R.O.W.; Methodology and Investigation, C.Z.; Data Analysis and Curation, C.Z., A.H., and S.T.; Writing – C.Z. and R.O.W.

DECLARATION OF INTERESTS

The authors declare no competing interests.

INCLUSION AND DIVERSITY

We worked to ensure sex balance in the selection of non-human subjects.

Received: May 31, 2022
Revised: August 11, 2022
Accepted: August 23, 2022
Published: September 16, 2022

REFERENCES

Bishop, D., Nikic, I., Kerschensteiner, M., and Misgeld, T. (2014). The use of a laser for correlating light and electron microscopic images in thick tissue specimens. Methods Cell Biol. *124*, 323–337. https://doi.org/10.1016/B978-0-12-801075-4.00015-X.

Briggman, K.L., Helmstaedter, M., and Denk, W. (2011). Wiring specificity in the direction-selectivity circuit of the retina. Nature *471*, 183–188. https://doi.org/10.1038/nature09818.

Cao, Y., Sarria, I., Fehlhaber, K.E., Kamasawa, N., Orlandi, C., James, K.N., Hazen, J.L., Gardner, M.R., Farzan, M., Lee, A., et al. (2015). Mechanism for selective synaptic wiring of rod photoreceptors into the retinal circuitry and its role in vision. Neuron *87*, 1248–1260. https://doi.org/10.1016/j.neuron.2015.09.002.

Cao, Y., Wang, Y., Dunn, H.A., Orlandi, C., Shultz, N., Kamasawa, N., Fitzpatrick, D., Li, W., Zeitz, C., Hauswirth, W., and Martemyanov, K.A. (2020). Interplay between cell-adhesion molecules governs synaptic wiring of cone photoreceptors. Proc. Natl. Acad. Sci. USA *117*, 23914–23924. https://doi.org/10.1073/pnas.2009940117.

Cardona, A., Saalfeld, S., Schindelin, J., Arganda-Carreras, I., Preibisch, S., Longair, M., Tomancak, P., Hartenstein, V., and Douglas, R.J. (2012). TrakEM2 software for neural circuit reconstruction. PLoS One *7*, e38011. https://doi.org/10.1371/journal.pone.0038011.

Chun, M.H., Han, S.H., Chung, J.W., and Wässle, H. (1993). Electron microscopic analysis of the rod pathway of the rat retina. J. Comp. Neurol. *332*, 421–432. https://doi.org/10.1002/cne.903320404.

Della Santina, L., Kuo, S.P., Yoshimatsu, T., Okawa, H., Suzuki, S.C., Hoon, M., Tsuboyama, K., Rieke, F., and Wong, R.O.L. (2016). Glutamatergic monopolar interneurons provide a novel pathway of excitation in the mouse retina. Curr. Biol. *26*, 2070–2077. https://doi.org/10.1016/j.cub.2016.06.016.

Ding, H., Smith, R.G., Poleg-Polsky, A., Diamond, J.S., and Briggman, K.L. (2016). Species-specific wiring for direction selectivity in the mammalian retina. Nature *535*, 105–110. https://doi.org/10.1038/nature18609.

Dunn, F.A., DellaSantina, L., Parker, E.D., and Wong, R.O.L. (2013). Sensory experience shapes the development of the visual system's first synapse. Neuron *80*, 1159–1166. https://doi.org/10.1016/j.neuron.2013.09.024.

Dunn, F.A., and Wong, R.O.L. (2014). Wiring patterns in the mouse retina: collecting evidence across the connectome, physiology and light microscopy. J. Physiol. *592*, 4809–4823. https://doi.org/10.1113/jphysiol.2014.277228.

Euler, T., Haverkamp, S., Schubert, T., and Baden, T. (2014). Retinal bipolar cells: elementary building blocks of vision. Nat. Rev. Neurosci. *15*, 507–519. https://doi.org/10.1038/nrn3783.

Freed, M.A., Smith, R.G., and Sterling, P. (1987). Rod bipolar array in the cat retina: pattern of input from rods and GABA-accumulating amacrine cells. J. Comp. Neurol. *266*, 445–455. https://doi.org/10.1002/cne.902660310.

Gamlin, C.R., Zhang, C., Dyer, M.A., and Wong, R.O.L. (2020). Distinct developmental mechanisms act independently to shape biased synaptic divergence from an inhibitory neuron. Curr. Biol. *30*, 1258–1268.e2. https://doi.org/10.1016/j.cub.2020.01.080.

Gray, E.G. (1969). Electron microscopy of excitatory and inhibitory synapses: a brief review. Prog. Brain Res. *31*, 141–155. https://doi.org/10.1016/S0079-6123(08)63235-5.

Grimes, W.N., Hoon, M., Briggman, K.L., Wong, R.O., and Rieke, F. (2014). Cross-synaptic synchrony and transmission of signal and noise across the mouse retina. Elife *3*, e03892. https://doi.org/10.7554/eLife.03892.

Grimes, W.N., Songco-Aguas, A., and Rieke, F. (2018). Parallel processing of rod and cone signals: retinal function and human perception. Annu. Rev. Vis. Sci. *4*, 123–141. https://doi.org/10.1146/annurev-vision-091517-034055.

Grimes, W.N., Zhang, J., Graydon, C.W., Kachar, B., and Diamond, J.S. (2010). Retinal parallel processors: more than 100 independent microcircuits operate within a single interneuron. Neuron *65*, 873–885. https://doi.org/10.1016/j.neuron.2010.02.028.

Grünert, U., and Martin, P.R. (1991). Rod bipolar cells in the macaque monkey retina: immunoreactivity and connectivity. J. Neurosci. *11*, 2742–2758.

Hartveit, E. (1999). Reciprocal synaptic interactions between rod bipolar cells and amacrine cells in the rat retina. J. Neurophysiol. *81*, 2923–2936. https://doi.org/10.1152/jn.1999.81.6.2923.

Hoon, M., Okawa, H., Della Santina, L., and Wong, R.O.L. (2014). Functional architecture of the retina: development and disease. Prog. Retin. Eye Res. *42*, 44–84. https://doi.org/10.1016/j.preteyeres.2014.06.003.

Kano, M., and Watanabe, T. (2019). Developmental synapse remodeling in the cerebellum and visual thalamus. F1000Res *8*. https://doi.org/10.12688/f1000research.18903.1.

Keeley, P.W., and Reese, B.E. (2010). Role of afferents in the differentiation of bipolar cells in the mouse retina. J. Neurosci. *30*, 1677–1685. https://doi.org/10.1523/JNEUROSCI.5153-09.2010.

Kolb, H., and Famiglietti, E.V. (1974). Rod and cone pathways in the inner plexiform layer of cat retina. Science *186*, 47–49. https://doi.org/10.1126/science.186.4158.47.

Liang, L., and Chen, C. (2020). Organization, function, and development of the mouse retinogeniculate synapse. Annu. Rev. Vis. Sci. *6*, 261–285. https://doi.org/10.1146/annurev-vision-121219-081753.

Maddox, J.W., Randall, K.L., Yadav, R.P., Williams, B., Hagen, J., Derr, P.J., Kerov, V., Della Santina, L., Baker, S.A., Artemyev, N., et al. (2020). A dual role for Cav1.4 Ca(2+) channels in the molecular and structural organization of the rod photoreceptor synapse. Elife *9*, e62184. https://doi.org/10.7554/eLife.62184.

Marquardt, T., Ashery-Padan, R., Andrejewski, N., Scardigli, R., Guillemot, F., and Gruss, P. (2001). Pax6 is required for the multipotent state of retinal progenitor cells. Cell *105*, 43–55. https://doi.org/10.1016/s0092-8674(01)00295-1.

Masland, R.H. (2012). The neuronal organization of the retina. Neuron *76*, 266–280. https://doi.org/10.1016/j.neuron.2012.10.002.

Massey, S.C., Mills, S.L., and Marc, R.E. (1992). All indoleamine-accumulating cells in the rabbit retina contain GABA. J. Comp. Neurol. *322*, 275–291. https://doi.org/10.1002/cne.903220213.

Morgan, J.L., Soto, F., Wong, R.O.L., and Kerschensteiner, D. (2011). Development of cell type-specific connectivity patterns of converging excitatory axons in the retina. Neuron *71*, 1014–1021. https://doi.org/10.1016/j.neuron.2011.08.025.

Nelson, R., and Kolb, H. (1985). A17: a broad-field amacrine cell in the rod system of the cat retina. J. Neurophysiol. *54*, 592–614. https://doi.org/10.1152/jn.1985.54.3.592.

Nériec, N., and Desplan, C. (2016). From the eye to the brain: development of the Drosophila visual system. Curr. Top. Dev. Biol. *116*, 247–271. https://doi.org/10.1016/bs.ctdb.2015.11.032.

Okawa, H., Della Santina, L., Schwartz, G.W., Rieke, F., and Wong, R.O.L. (2014). Interplay of cell-autonomous and nonautonomous mechanisms tailors synaptic connectivity of converging axons in vivo. Neuron *82*, 125–137. https://doi.org/10.1016/j.neuron.2014.02.016.

Pourcho, R.G., and Goebel, D.J. (1985). A combined Golgi and autoradiographic study of (3H)glycine-accumulating amacrine cells in the cat retina. J. Comp. Neurol. *233*, 473–480. https://doi.org/10.1002/cne.902330406.

Raviola, E., and Dacheux, R.F. (1987). Excitatory dyad synapse in rabbit retina. Proc. Natl. Acad. Sci. USA *84*, 7324–7328. https://doi.org/10.1073/pnas.84.20.7324.

Sandell, J.H., Masland, R.H., Raviola, E., and Dacheux, R.F. (1989). Connections of indoleamine-accumulating cells in the rabbit retina. J. Comp. Neurol. *283*, 303–313. https://doi.org/10.1002/cne.902830210.

Sanes, J.R., and Zipursky, S.L. (2020). Synaptic specificity, recognition molecules, and assembly of neural circuits. Cell *181*, 1434–1435. https://doi.org/10.1016/j.cell.2020.05.046.

Schubert, T., Kerschensteiner, D., Eggers, E.D., Misgeld, T., Kerschensteiner, M., Lichtman, J.W., Lukasiewicz, P.D., and Wong, R.O.L. (2008). Development of presynaptic inhibition onto retinal bipolar cell axon terminals is subclass-specific. J. Neurophysiol. *100*, 304–316. https://doi.org/10.1152/jn.90202.2008.

Sinha, R., Siddiqui, T.J., Padmanabhan, N., Wallin, J., Zhang, C., Karimi, B., Rieke, F., Craig, A.M., Wong, R.O., and Hoon, M. (2020). LRRTM4: a novel regulator of presynaptic inhibition and ribbon synapse arrangements of retinal bipolar cells. Neuron *105*, 1007–1017.e5. https://doi.org/10.1016/j.neuron.2019.12.028.

Steinecke, A., Hozhabri, E., Tapanes, S., Ishino, Y., Zeng, H., Kamasawa, N., and Taniguchi, H. (2017). Neocortical chandelier cells developmentally shape axonal arbors through reorganization but establish subcellular synapse specificity without refinement. eNeuro *4*. ENEURO.0057, 17.2017. https://doi.org/10.1523/ENEURO.0057-17.2017.

Sterling, P., and Matthews, G. (2005). Structure and function of ribbon synapses. Trends Neurosci. *28*, 20–29. https://doi.org/10.1016/j.tins.2004.11.009.

Strettoi, E., Dacheux, R.F., and Raviola, E. (1990). Synaptic connections of rod bipolar cells in the inner plexiform layer of the rabbit retina. J. Comp. Neurol. *295*, 449–466. https://doi.org/10.1002/cne.902950309.

Tsukamoto, Y., Morigiwa, K., Ueda, M., and Sterling, P. (2001). Microcircuits for night vision in mouse retina. J. Neurosci. *21*, 8616–8623.

Tsukamoto, Y., and Omi, N. (2017). Classification of mouse retinal bipolar cells: type-specific connectivity with special reference to rod-driven AII amacrine pathways. Front. Neuroanat. *11*, 92. https://doi.org/10.3389/fnana.2017.00092.

Wässle, H. (2004). Parallel processing in the mammalian retina. Nat. Rev. Neurosci. *5*, 747–757. https://doi.org/10.1038/nrn1497.

Xu, C., Theisen, E., Maloney, R., Peng, J., Santiago, I., Yapp, C., Werkhoven, Z., Rumbaut, E., Shum, B., Tarnogorska, D., et al. (2019). Control of synaptic specificity by establishing a relative preference for synaptic partners. Neuron *103*, 865–877.e7. https://doi.org/10.1016/j.neuron.2019.06.006.

Yan, W., Laboulaye, M.A., Tran, N.M., Whitney, I.E., Benhar, I., and Sanes, J.R. (2020). Mouse retinal cell atlas: molecular identification of over sixty amacrine cell types. J. Neurosci. *40*, 5177–5195. https://doi.org/10.1523/JNEUROSCI.0471-20.2020.

Yoshimatsu, T., Williams, P.R., D'Orazi, F.D., Suzuki, S.C., Fadool, J.M., Allison, W.T., Raymond, P.a., and Wong, R.O. (2014). Transmission from the dominant input shapes the stereotypic ratio of photoreceptor inputs onto horizontal cells. Nat. Commun. *5*, 3699. https://doi.org/10.1038/ncomms4699.

Zhang, C., Kolodkin, A.L., Wong, R.O., and James, R.E. (2017). Establishing wiring specificity in visual system circuits: from the retina to the brain. Annu. Rev. Neurosci. *40*, 395–424. https://doi.org/10.1146/annurev-neuro-072116-031607.

STAR★METHODS

KEY RESOURCES TABLE

REAGENT or RESOURCE	SOURCE	IDENTIFIER
Chemicals, peptides, and recombinant proteins		
Ames' medium	Sigma	Cat.# A1420
Vectashield	Vector Laboratories	Cat# H-1000, RRID: AB_2336789
Experimental models: Organisms/strains		
Mouse: C57BL/6	The Jackson Laboratory	Strain #:000664 RRID:IMSR_JAX:000664
Mouse: αPax6-Cre	Guillermo Oliver	RRID:MGI:6111814
Mouse: Grm6-YFP-STOP-DTA	Rachel Wong	N/A
Software and algorithms		
Fiji	NIH	https://fiji.sc/, RRID: SCR_002285
Amira	Thermo Fisher Scientific	https://www.fei.com/software/amira/, RRID: SCR_014305
Prism	GraphPad	https://www.graphpad.com/scientific-software/prism/, RRID: SCR_002798

RESOURCE AVAILABILITY

Lead contact

Further information and requests for resources and reagents should be directed to and will be fulfilled by the lead contact, Rachel O.L. Wong (wongr2@uw.edu).

Materials availability

This study did not generate new unique reagents.

Data and code availability

- The EM datasets collected in the current study have not been deposited into a public repository because of the scale of the datasets and use in ongoing studies but are available from the lead contact upon request.
- This paper does not report original code.
- Any additional information required to reanalyze the data reported in this paper is available from the lead contact upon request.

EXPERIMENTAL MODEL AND SUBJECT DETAILS

Mice

All procedures were conducted in accordance with University of Washington Institutional Animal Care and Use Committee guidelines. C57BL/6 (wildtype, WT) mice were purchased from Jackson Laboratory (JAX Stock No. 000664). *αPax6-Cre* mice were obtained from Guillermo Oliver (Northwestern University) (Marquardt et al., 2001). *Grm6-YFP-STOP-DTA* mice were generated as described previously (Morgan et al., 2011). Female *αPax6-Cre* mice were crossed with male *Grm6-YFP-STOP-DTA* mice to generate *αPax6-Cre x Grm6-YFP-STOP-DTA* (DTA) mice (Okawa et al., 2014) for this study. Mice of both sexes at postnatal day (P)7–60 were used.

METHOD DETAILS

Retinal tissue preparation and fixation

Mice were euthanized with Isoflurane (5%), cervically dislocated or decapitated, and enucleated. Retinas were dissected at room temperature in Ames' medium (Sigma) bubbled with 95%O_2/5%CO_2. For light

microscopy, retinas were mounted flat, ganglion cell side up, onto filter paper (Millipore), and the tissue was subsequently fixed with 4% paraformaldehyde for 15 min at room temperature. For correlative light and electron microscopy, retinas mounted on filter paper were fixed with 2–4% glutaraldehyde in 0.1M sodium cacodylate buffer (pH7.4) for 15–30 min at room temperature. For electron microscopy only, retinal pieces were fixed with 4% glutaraldehyde in 0.1M sodium cacodylate buffer for 30 min to 1 h at room temperature and overnight at 4°C.

Confocal image acquisition and processing

Fluorescence images were acquired on a TCS LSP8 confocal microscope (Leica), using a 0.75 numerical aperture (NA) 20× oil objective lens. Images were acquired at an x-y resolution of 1.5 μm/pixel and z step of 2 μm. Adjustment of contrast, brightness and hue, and maximum intensity projections were all performed using Fiji (NIH).

Correlative light and electron microscopy

The fixed retinal samples (as described above) were washed and mounted under a coverglass in 0.1M sodium cacodylate buffer for two-photon imaging. Specifically, areas with sparse YFP-positive rod bipolar cells (RBCs) were identified under a Ti:sapphire laser (Spectra-Physics). Fiduciary marks were burned into the tissue by the laser around the cell clusters using the near-infrared branding (NIRB) method (Bishop et al., 2014). Subsequently, the retinas were unmounted and fixed in 4% glutaraldehyde overnight for electron microscopy.

Serial block-face scanning electron microscopy (SBFSEM)

Retinal samples were prepared for the SBFSEM as described previously (Della Santina et al., 2016). Samples were sectioned and imaged on a 3View SEM microscope (Zeiss) or a VolumeScope SEM (Thermo Fisher Scientific), at a voxel size of 5 × 5 × 50 nm^3 or 6 × 6 × 50 nm^3. In this study, we obtained EM micrographs including the full depth of the inner plexiform layer (IPL) from WT (1 adult, 1 P7, and 2 P9) and DTA (1 adult and 1 P10) retinas. We also used image stacks acquired from previous studies for our analysis, including an adult (Ding et al., 2016) and a P11 wildtype (Gamlin et al., 2020). The approximal volumes of each image stack are as follows: adult WTs (1,412,000 and 2,730,000 μm^3), P7 WT (428,000 μm^3), P9 WTs (1,017,000 and 2,188,000 μm^3), P11 WT (419,000 μm^3), adult DTA (562,000 μm^3), and P10 DTA (645,000 μm^3).

Image reconstruction and analysis

EM micrographs were aligned using TrakEM2 (Cardona et al., 2012) in Fiji (NIH). The processes and somata of cells were manually traced and segmented using the AreaTree function, and synapses and varicosities were annotated using the AreaList function of TrakEM2. RBC axons were identified by their morphology and stratification level at the most inner IPL (Tsukamoto and Omi, 2017; Wässle, 2004). To reconstruct A17 ACs, we identified their processes by their characteristic reciprocal synapse at RBC synaptic dyads (Grimes et al., 2014; Sinha et al., 2020), and then traced the processes to the cell body and then the arbor. Ribbon synapses and inhibitory synapses were identified according to previously reported features to determine connectivity (Gray, 1969; Sterling and Matthews, 2005). The types/classes of A17 synaptic partners were determined by their morphology and synapse specializations as described previously (Gamlin et al., 2020). The visualization of volume reconstructions was performed in Amira (Thermo Fisher Scientific).

QUANTIFICATION AND STATISTICAL ANALYSIS

Statistical analyses were performed using Prism (GraphPad). Distributions of each parameter were tested for normality using the D'Agostino and Pearson omnibus test and appropriate parametric or non-parametric statistical analyses were applied. Unpaired t-test or Mann-Whitney test was performed to compare parameters between different ages or genotypes. One-way analysis of variance (ANOVA) test or Kruskal-Wallis test was performed to compare the same parameter across more than two ages. Statistical parameters including the value of n, mean ± SEM, and statistical significance are provided in the text or figure legends. Significance was Fdetermined at $p < 0.05$.